Pis'ma v ZhETF, vol. 82, iss. 5, pp. 312 – 316

Identifying the electronic properties of the Ge(111)-(2×1) surface by low temperature scanning tunneling microscopy

*P. I. Arseyev, N. S. Maslova**, *V. I. Panov**, *S. V. Savinov**[1)], *C. Van Haesendonck*[+]

P.I. Lebedev Physical Institution RAS, 119991 Moscow, Russia

**Department of Physics, Moscow State University, 119992 Moscow, Russia*

[+]*Laboratory of Solid-State Physics and Magnetism, K.U.Leuven, B-3001 Leuven, Belgium*

Submitted 6 July 2005

We present the results of our low temperature scanning tunneling microscopy (STM) investigation of the clean Ge(111) surface. Our experiments enable the first time STM observation of one-dimensional surface screening around surface defects. We identify the dominating role of surface states in the low temperature STM imaging as well as the important influence of non-equilibrium kinetics on the measured tunneling spectra.

PACS: 68.35.Dv, 68.37.Ef, 73.20.At

The (111) surface of Ge is among the most widely studied elementary semiconductor surfaces. Some features of this surface are presently well established, e.g., the (2×1) surface reconstruction corresponding to a π-bonded chain model with buckling [1 – 3]. On the other hand, some of the properties still remain to be clarified. There is no clear understanding of the (2×1) reconstructed surface electronic properties, which should somehow reveal a one-dimensional (1D) character. In this work we present the results of our low temperature scanning tunneling microscopy (STM) investigation of clean Ge(111)-(2×1) surfaces [4]. The samples under investigation were cut from heavily doped (resistivity $1\,\mathrm{m}\Omega\cdot\mathrm{cm}$) Ge single crystals with n-type bulk conductivity. The doping element was phosphorus, which is a shallow impurity with an ionization energy of 13 meV, while the doping concentration was rather high around $8\cdot 10^{18}\,\mathrm{cm}^{-3}$. The samples were $1.5\times 1.5\times 3.0\,\mathrm{mm}^3$ slabs with the long axis aligned along the [111] direction. Samples are cleaved *in situ* after the low temperature STM instrument is cooled down to liquid helium temperature. The details of the cleaving procedure and the experimental STM setup are described elsewhere [4]. After cleavage a high quality Ge(111) surface with pronounced optical reflectivity (mirror) is exposed to the STM tip for imaging and spectroscopy.

According to the commonly accepted point of view, the Ge(111) surface with (2×1) reconstruction is terminated by π-bonded chains with Ge atoms running along the $[01\bar{1}]$ direction [2] and only every second atomic chain is imaged as a protrusion by STM. The surface unit cell contains two atoms, both having one dangling bond, and these bonds are responsible for π-bonding along zigzag rows. One atom (*up*-atom) is shifted out of the surface, while the other atom (*down*-atom) is shifted towards the surface. Consequently, the bonding surface states band π_{VB} derived from the *up*-atom orbital is filled, while the anti-bonding surface states band π^*_{CB} derived from the *down*-atom orbital is empty. At sufficiently high doping concentration the anti-bonding surface states band π^*_{CB} is partially populated and at the surface the Fermi level lies above the bottom of the π^*_{CB} band. The band structure for a heavily doped n-type Ge(111)-(2×1) surface, which is consistent with first principles calculations [5], photoemission measurements [6] and our local tunneling spectroscopy data (see below), is illustrated in Fig.1. Here we would like to mention some numbers characteristic for Ge(111)-(2×1) surface. The widths of anti-bonding π^*_{CB} and bonding π_{VB} surface states bands which can be derived from both theoretical [5] and experimental [6] data approximately equal to 1.2 and 0.8 eV respectively. The value of the band gap on the surface E_{GS} measured by means of scanning tunneling spectroscopy at low temperature [7] is about 0.5 eV. The bulk band gap [8] equals to 0.74 eV at liquid helium temperature (4.2 K).

Typical STM images of the Ge(111)-(2×1) surface are presented in Fig.2 for different values of the tunneling bias voltage applied to the sample (tip is grounded), which implies that filled (empty) state images are taken at negative (positive) bias. The first two images in Fig.2 were acquired with a bias voltage corresponding to the band gap region. All images reveal an ordered, chain-like surface structure. For the Ge(111) surface such a

[1)]e-mail: SavinovSV@mail.ru

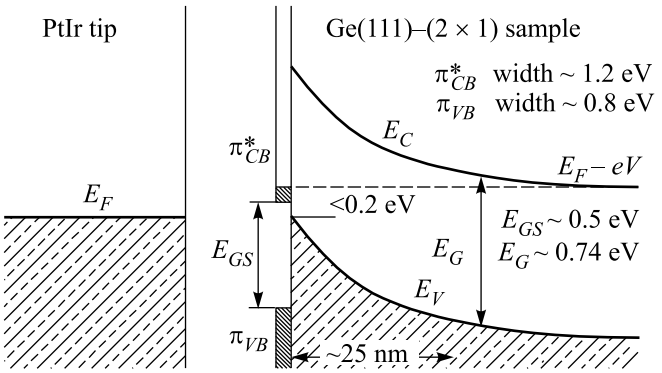

Fig.1. Band structure of the metal tip – Ge(111)-(2×1) tunneling junction. π_{VB} and π^*_{CB} denote the bonding and anti-bonding surface states band, respectively. The partially filled surface states anti-bonding (conduction) band is responsible for Fermi level pinning in the vicinity of the valence band maximum. The surface (E_{GS}) and bulk (E_G) band gaps are indicated. The figure is not to scale

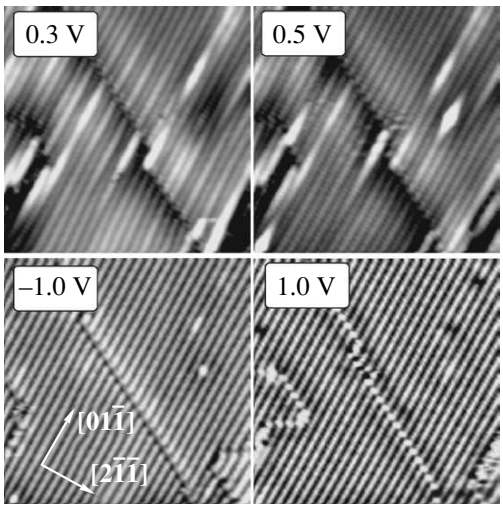

Fig.2. STM images of the Ge(111)-(2×1) surface for different sample bias voltage. The set point for the tunneling current is 20 pA. The image size is 14 nm × 14 nm

chain-like structure has been attributed to a (2×1) surface reconstruction with π-bonded chains [2]. The images in Fig.2 reveal the presence of surface defects, including the presence of ad-atoms on the surface.

We now turn to some remarkable features appearing in the Ge(111)-(2×1) surface STM images shown in Fig.2. First, the images taken with a bias voltage corresponding to the band gap reveal the presence of screening of localized surface charges. The streaks observed in the STM images reflects the perturbation of the local density of states by the scattering on surface imperfections of electrons with 1D confinement along the π-bonded chain rows. STM images of all surface defects (impurities, ad-atoms, atomic size elements of domain boundaries) have a pronounced 1D shape. The areas around the defects appear as stripes with length up to 60 Å along the direction of the π-bonded chain rows ([01$\bar{1}$] direction), while their width approximately equals the period of the surface reconstruction in the [2$\bar{1}\bar{1}$] direction (about 7 Å). For an asymmetric defect such as a single atomic size element of a domain boundary, the stripe, which reflects the screening in the STM image, is asymmetric along the chain rows. While the screening cloud is localized mainly next to the defect, it smoothly decays in one direction with increasing distance from the domain boundary, but in the opposite direction it abruptly ends at the domain boundary. For symmetric defects such as individual surface impurity atoms or ad-atoms, the screening cloud has a symmetric shape along the chain row. We would like to stress that the contrast of the empty states STM images (positive sample bias voltages) is higher than for the filled states STM images (negative sample bias voltages). This can be accounted for by the different screening for empty and filled states, respectively (see below). It is also important to note that the low temperature STM images of the Ge(111)-(2×1) surface become completely dominated by the density of surface electronic states for the range of bias voltages corresponding to the surface band gap.

We also experimentally probed the local density of electronic states. The results of scanning tunneling spectroscopy (STS) measurements are presented in Fig.3. The normalized tunneling conductivity spectra were obtained by averaging of the experimental data collected above a square surface area containing four π-bonded zigzag rows. The details of the data treatment procedure are described elsewhere [9]. The overall energy resolution for the present experiments is estimated to be 20 meV due to our numerical method of differentiation and subsequent averaging. This value is sufficiently small for reliable tunneling spectroscopy on semiconductors.

Let us now point out the important features of the spectroscopic measurements on the Ge(111)-(2×1) atomically flat surface at low temperature. The presence of a band gap can be observed in the spectrum with bottom and top located at −0.07 V and +0.5 V, respectively. The Fermi level (0 V on the V-axis) is positioned in the spectrum slightly above the valence band maximum, although our samples are heavily doped and have n-type bulk conductivity. This can be accounted for by Fermi level pinning at the surface in case of the Ge(111)-(2×1) surface (see Fig.1). It is interesting to note that for the Ge(111)-(2×1) surface the position of the Fermi

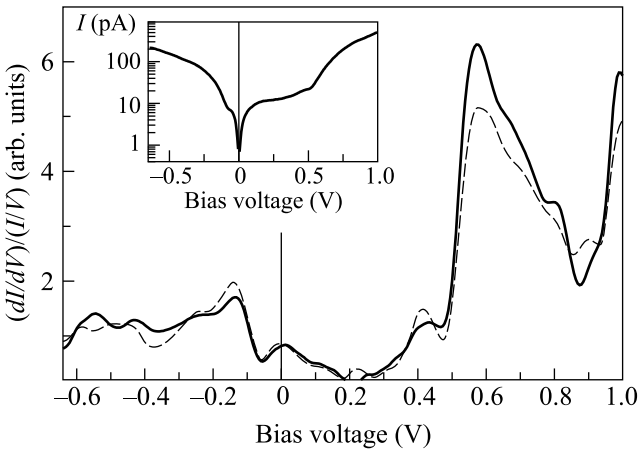

Fig.3. $(dI/dV)/(I/V)$ normalized tunneling conductivity measured above two different defect free areas of the Ge(111)-(2×1) surface as a function of the applied bias voltage. The inset shows the logarithm of the current-voltage characteristic $I(V)$. The current set point for the measurements is $I_t = 20\,\text{pA}$, while the voltage for the approach is $V_t = 0.3\,\text{V}$

level in the tunneling spectra remains the same, independent of the type of doping of the bulk semiconductor, i.e, p-type or n-type bulk conductivity [10]. According to photoemission data the position is independent of the bulk doping concentration as well [6]. The main source of the difference in tunneling spectra for the p-type and n-type Ge(111)-(2×1) surface is the difference in surface band bending. While for a n-type sample surface band bending almost exceeds the bulk band gap value (Fig.1), bands remain nearly flat near a p-type sample surface.

The tunneling current inside the bang gap is not negligible (see inset in Fig.3). With our choice of the set point for the tunneling current ($I_t = 20\,\text{pA}$) a comparable value of the tunneling current was detected throughout the band gap, except for a narrow region ($|V| < 0.1\,\text{V}$) around the Fermi level. This implies that the surface states are able to carry a current up to $\sim 10^9$ electrons per second. Hence, the tunneling rate through surface states is comparable to the relaxation rate of non-equilibrium electrons due to the electron-phonon interaction at low temperature ($10^8\,\text{s}^{-1}$ [11]). A local non-equilibrium charge can then be accumulated on the surface states, causing local band bending. This bending alters the ratio of the tunneling rates from surface states to the bulk semiconductor and to the metallic tip, respectively, and consequently alters the *measured* tunneling spectrum.

As can be seen from Fig.3, the tunneling conductivity curve reaches an absolute minimum about 0.2 V above the Fermi level. Two other local minima followed by peaks are located on both sides of the surface band gap. A relatively weak peak is centered at −0.15 V near the valence band maximum. A strong peak with two shoulders on the high energy side can be found at 0.6 V, just below the conduction band minimum. The dips appearing at the band gap edges are characteristic for our experiments and are highly reproducible.

In order to understand the obtained experimental results we rely on a model of resonant tunneling trough surface states bands. The details of this model can be found in [12]. When the bias voltage is in the voltage range corresponding to the band gap, the coupling between surface and bulk states is very weak. As indicated in Fig.1, a 250 Å wide depletion layer is separating the surface and bulk states. This depletion layer is formed because of charging of the surface states, which results in strong band bending near the surface. For heavy doping the Ge(111)-(2×1) surface band bending almost exceeds the band gap value (see Fig.1). Consequently, a correct modeling of the tunneling processes through surface states requires to treat the STM junction as a double barrier structure and tunneling through the depletion layer needs to be taken into account.

Using the non-equilibrium Keldysh Green's function formalism the local tunneling current can be determined [12]:

$$I(V,\mathbf{r}) = \int d\varepsilon\, \nu(\varepsilon,\mathbf{r})\,[n_t^0(\varepsilon) - n_b^0(\varepsilon)]\,\frac{\gamma_t(\varepsilon)\gamma_b(\varepsilon)}{\gamma_t(\varepsilon)+\gamma_b(\varepsilon)},$$

where γ_t and γ_b are the tunneling rates from the surface states band to the metallic tip and to the bulk semiconductor, respectively. n_t^0 and n_b^0 are the equilibrium filling numbers of the metallic tip and the semiconductor, respectively, and $\nu(\varepsilon,\mathbf{r})$ is the local density of surface states. It is important to note that $\nu(\varepsilon,\mathbf{r})$ *is not* the density of defect free surface states, but it includes the contribution from surface defects of all kinds (impurity atoms, lattice vacancies, etc.).

We now turn in more detail to specific features of the tunneling current in the vicinity of a defect or individual impurity atom for small positive sample bias voltages. Because the empty surface states π^*_{CB} band is partially filled, the impurity potential is screened by surface electrons:

$$W_{imp}(\mathbf{q}) = \frac{W_0(\mathbf{q})}{\varepsilon(\mathbf{q},0)},$$

where $\varepsilon(\mathbf{q},0)$ is the dielectric function of the semiconductor surface states band. The density of empty surface states is changed by this screened potential. $\varepsilon(\mathbf{q},0)$ has a logarithmic singularity at $q = 2k_F$. When the Fermi level falls inside the empty surface states band π^*_{CB},

the screening effects become more pronounced within the range of positive sample bias when compared to the cases of low doped n-type and p-type surfaces for which the π^*_{CB} band is completely empty. Consequently, the empty states STM images of highly doped n-type samples reveal details caused by local screening in contrast to STM images of p-type samples, where empty states STM images are less informative than filled states images.

Because of the spatial localization of surface states in the π-bonded chains, the screening occurs in the direction of π-bonded atomic rows, and consequently it is a quasi 1D process. The additional contribution to the local surface density of states due to screening of the impurity potential can be expressed as

$$\delta\nu = \frac{W\nu_0^2}{1 - W\nu_0} \sin(2\mathbf{k}(\varepsilon)\cdot\mathbf{r} + \delta),$$

where ν_0 is the unperturbed density of surface states, δ is the phase shift determined by the exact shape of the potential and $\mathbf{k}(\varepsilon)$ is the quasi 1D wave vector corresponding to the energy value ε. The additional term for the tunneling current at small positive bias voltage can then be written as

$$I(V,r) = \frac{e^2}{\hbar} V \frac{W\nu_0^2}{1 - W\nu_0} \frac{\gamma_t(\varepsilon_F)\gamma_b(\varepsilon_F)}{\gamma_t(\varepsilon_F) + \gamma_b(\varepsilon_F)} \frac{\cos(2k_F r + \delta)}{k_F r},$$

where e is the electron charge and $\hbar$ is Plank's constant.

In the effective mass approximation the Fermi level position is determined by the expression

$$\varepsilon_F = \frac{\hbar^2 k_F^2}{2\, m_{\text{eff}}}.$$

As can be inferred from the experimental observations presented in Fig.2, the typical spatial extent of the area with enhanced tunneling current near a defect is about 50 Å. We suppose that it is reasonable to use the bulk value of electron effective mass: $m_{\text{eff}} = 0.063\, m$ with m the free electron mass. In this case the degree of occupation for the empty surface states band can be estimated from the value of the Fermi wavelength $k_F^{-1} \sim 100$ Å, and we then find that the Fermi level ε_F is approximately 4 meV *above* the bottom of the π^*_{CB} band, which is close to the value of 0.5% band filling obtained in [13].

We argue that specific features of the surface electronic structure do not dramatically affect the general shape of the tunneling spectrum. E.g., our experimental tunneling conductivity spectrum for the Ge(111)-(2×1) surface is *very* similar to the tunneling spectrum for the Ge(111)-c(2×8) surface [14], i.e, the exact type of surface reconstruction *does not* dominate the tunneling spectrum. When the applied bias voltage approaches the conduction band from the bottom, the tunneling rate from surface states to semiconductor bulk states increases (Fig.1) due to a decrease of the depletion layer width. At a certain voltage this tunneling rate becomes comparable to the tunneling rate from surface states to the metallic tip. The weakest link of the STM junction, which is caused by tunneling from surface states to the bulk semiconductor, will then disappear. One may expect in this specific range of bias voltages the appearance of a peak in the tunneling conductivity versus bias voltage dependence [15]. Because the onset of the peak is located *inside* the surface band gap, the value of the surface band gap *measured* by tunneling spectroscopy is smaller than its real value.

The difference between tunneling spectroscopy on Ge(111)-(2×1) and Ge(111)-c(2×8) surfaces is due to the difference in the physics of the depletion layer formation. In case of n-type Ge(111)-(2×1) strong band bending is present at the surface due to charging of the surface states. On the other hand, tip induced band bending is responsible for the creation of the depletion layer at the Ge(111)-c(2×8) surface [14].

The bulk band gap value for the Ge(111)-(2×1) surface is 0.74 eV [8]. Due to the gap narrowing described above, the surface band gap value derived from our experimental tunneling conductivity spectra is about 0.6 eV (see Fig.1). This value corresponds to the reduced bulk band gap value, and not to the separation between the surface states related bands. We would like to point out once more that, in spite of the dominating role of surface states in low temperature STM imaging of the (111) surface of elemental semiconductors, the STS spectra always reflect the electronic structure of *bulk* states.

The intense peak appearing in the tunneling conductivity spectra near the conduction band edge is a characteristic feature of spectroscopy on the (111) surface of Ge and Si that is not strongly affected by the exact type of reconstruction (2×1, 2×8) [14, 16].

In conclusion, the Ge(111)-(2×1) surface obtained by *in situ* sample cleavage was investigated by means of low temperature STM and STS. The dominating influence of surface states on the STM image formation was revealed. It was shown that perturbations of the local density of states around surface defects are confined along the π-bonded chain rows, directly reflecting the quasi 1D spatial distribution of the surface states. The surface band structure for the heavily doped n-type Ge(111)-(2×1) surface was clarified and the degree of occupation of the empty surface states band π^*_{CB} was estimated from the typical spatial extent of the area with enhanced tunneling current. It was demonstrated that

the tunneling spectrum is determined not only by the local density of states, but also by the non-equilibrium kinetics of the tunneling processes.

The authors are grateful to A. Ezhov for technical assistance. This research was partially supported by RFBR grants # 03-02-16807 and # 04-02-19957 and by a grant for the Leading Scientific Schools (# 1604-2003-2). Support from the Samsung Corporation is also gratefully acknowledged. C.V.H would like to thank the Fund for Scientific Research – Flanders (Belgium) as well as the Belgian Interuniversity Attraction Poles (IAP) and the Flemish Concerted Action (GOA) research programs for additional financial support.

1. R. M. Tromp, L. Smith, and J. F. van der Veen, Phys. Rev. B **30**, 6235 (1984).
2. K. C. Pandey, Phys. Rev. Lett. **47**, 1913 (1981).
3. N. Takeuchi, A. Selloni, A. I. Shkrebtii, and E. Tosatti, Phys. Rev. B **44**, 13611 (1991).
4. S. I. Vasilev, S. I. Oreshkin, V. I. Panov et al., Instrum. and Experim. Technique **40**, 566 (1997).
5. M. Rohlfing, M. Palummo, G. Onida, and R. Del Sole, Phys. Rev. Lett. **85**, 5440 (2000).
6. J. N. Nicholls and B. Reihl, Surf. Sci. **218**, 237 (1989).
7. R. M. Feenstra, G. Meyer, F. Moresco, and K. H. Rieder, Phys. Rev. B **64**, 081306(R) (2001).
8. C. S. Wang and B. M. Klein, Phys. Rev. B **24**, 3393 (1981).
9. C. Van Haesendonck, N. S. Maslova, V. I. Panov et al., Int. J. of Nanoscience **2**, 575 (2003).
10. D. E. Eastman and J. L. Freeouf, Phys. Rev. Lett. **33**, 1601 (1974).
11. O. Agam, N. S. Wingreen, B. L. Altshuler et al., Phys. Rev. Lett. **78**, 1956 (1997).
12. P. I. Arseyev, N. S. Maslova, and S. V. Savinov, JETP Lett. **68**, 239 (1998).
13. J. N. Nicholls, P. Mårtensson, and G. V. Hansson, Phys. Rev. Lett **54**, 2363 (1985).
14. R. M. Feenstra, S. Gaan, G. Meyer, and K. H. Rieder, Phys. Rev. B **71**, 125316 (2005).
15. A. Depuydt, C. Van Haesendonck, N. S. Maslova et al., Phys. Rev. B **60**, 2619 (1999).
16. J. K. Garleff, M. Wenderoth, K. Sauthoff et al., Phys. Rev. B **70**, 245424 (2004).